ENGINEERING TRANSACTIONS • *Engng. Trans.* • **53**, 2, 197–229, 2005
Polish Academy of Sciences • Institute of Fundamental Technological Research
10.24423/engtrans.442.2005

EXPERIMENTAL ANALYSIS OF GRANULAR MATERIAL FLOWS USING THE TECHNIQUE OF DIGITAL PARTICLE IMAGE VELOCIMETRY

I. Sielamowicz

Białystok Technical University,
ul. Wiejska 45, 15-351 Białystok, Poland
e-mail: sieliren@pb.bialystok.pl

This paper presents the results of experiments of granular flows carried out for two configurations – in a plane model with vertical walls and in a wedge-shaped model. Both models were built of plexiglass and replicate the geometry of a silo. The flow processes of central and eccentric discharge were recorded by a high resolution camera (SensiCam) through the transparent walls of the models. PIV measurements allow to obtain the following data of the flow: the plug flow zone evolution, velocity magnitude contours, velocity fields, velocity distributions on certain levels in the models, traces of individual particles. Local deformations and stresses in the material may be also determined. The models were filled in a natural way through a pipe placed vertically in the symmetry axis above the models or through a sieve. In the case of the plane model, three cases of eccentric flows were investigated. Dynamic behaviour of the flowing materials recorded by the new measurement technique DPIV, commonly used in fluid mechanics, now applied for granular material flows, is analyzed. Uniform and repeatable packing of the materials with no particle segregation was obtained. Three different grain types were used in the experiments (amaranthus, flax-seed and buckwheat). These grains represent different physical properties and exhibit the phenomenon of static electricity of the materials when flowing and sliding over plexiglass.

1. Introduction

Experimental works carried in different laboratories are based on Jenike's investigations on modes of granular material flows in hoppers, published in [16, 17]. The fundamental mode is the radial velocity field (RVF) and the radial stress field (RSF) or next two types of flow – mass flow and funnel flow were the basic assumptions in these analyses.

This paper presents the application of a new measurement technique Digital Particle Image Velocimetry which enables recording of the range of stagnant boundaries in the flowing material and velocity fields, velocity magnitude contours, displacement fields, velocity distributions, traces of individual particles or calculation of stresses at the stagnant zone boundaries. An Optical Flow technique based on the use of Dynamic Programming [38] has been applied to Particle Image Velocimetry thus yielding a significant increase in the accuracy and spatial

resolution of the velocity field. The aim of the present investigation is to explore the possibility of using the optical flow technique based on PIV to measure the velocity in a granular flow. Particle Image Velocimetry (PIV) is a method used for two-dimensional flow structure evaluation. It enables the measurement of the instantaneous in-plane velocity field within a planar section of the flow field, the spatial gradients, dissipation of turbulent energy, spatial correlations, and the like. In [38] one can find a detailed description of the history, possibilities and development of PIV techniqe and the reasons for introducing an alternative approach – Digital Particle Image Velocimetry (DPIV). Despite recent progress in the DPIV development, further improvement of the accuracy and minimization of the computational time still remains a current research goal. One of the main drawbacks of classical DPIV was its inability to accurately resolve the flow regions characterized by large velocity gradients. But this limitation was removed by introducing by optical flow method as an interesting alternative, offering high evaluation accuracy. One of the first successful attempts to apply the PIV technique to granular matter was described by WATERS and DRESCHER in [49] and LUEPTOW *et al.* [21]. Recently OSTENDORF and SCHWEDES [33], SIELAMOWICZ and KOWALEWSKI [41], BÖHRNSEN *et al.* [7], SIELAMOWICZ and BŁOŃSKI [43] reported the use of the PIV technique in their experiments to obtain information on local velocities of particles at several elevations in the densely packed materials. OSTENDORF and SCHWEDES [34] combined PIV measurements with wall normal stresses measurements at different points of time in the large scale silo.

2. EXPERIMENTAL SETUP

A series of experiments was conducted in a plane flat-bottomed hopper model and in a wedge-shaped model, both made of plexiglass. The optical flow DPIV technique is used to record evolution of the flow. In the plane model central and eccentric flow was investigated with changing position of the outlet. In the wedge-shaped model behaviour of flowing grains was recorded for mass flow only.

Different velocity distributions form in the vicinity of the outlet and near the upper surface in the initial phase of the flow in the case of the central discharge. In the advanced phase of the flow, the flow zone widens and the boundaries become more or less curved. Unexpected flow patterns form during non-symmetrical filling and discharge. In fact, in practice the uncontrollable way of filling and discharge result in dynamic loads which may induce failure of the bin.

Figure 1 presents experimental setups used for the flow analysis. They consist of a plexiglass box, a set of illumination lamps, and a high resolution CCD camera (PCO SensiCam). The 12-bit pairs of images with resolution of 1280 pixels × 1024 pixels and maximum frequency of 3.75 Hz were acquired by Pentium 4 based personal computer. Long sequences of 100–400 images were taken

at variable time intervals for subsequent evaluation of the velocity fields. The velocity field was evaluated for triplets of images using optical flow PIV technique. In both cases, dense velocity fields with vectors for each pixel of the image were obtained and used for further evaluation of the velocity profiles, velocity contours and streamlines. A streamline is a term used in fluid mechanics. In granular material flows one should introduce a term – a trace of individual particles. Intrinsic resolution of the PIV technique is limited by the size of the area of interest that is used in the application of the cross-correlation algorithm between subsequent images and this is generally one order of magnitude larger than a single pixel. Here digital images are recorded directly with a CCD camera and frame-grabber, and can be studied without the unnecessary delay and overhead associated with the digitisation of photographs. DPIV allows a simple realization of the cross-correlation technique for pairs of two separate images. The typical DPIV evaluation procedure is based on the analysis of two successive images of the flow. A velocity vector is obtained for every pixel of the image. Calibration carried out for synthetic sequences of images shows that the accuracy of measured displacement is about 0.5 pixel/frame for tested two–image sequences and 0.2 pixel/frame for four-image sequences.

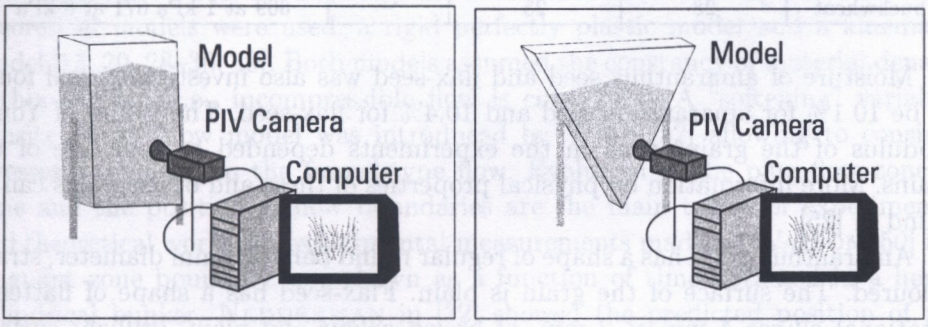

FIG. 1. Experimental setup for the plane and converging hopper models.

The plexiglass flat-bottomed silo model has a height of 80 cm, a depth of 10 cm, and a width of 26 cm. The model was placed on a stand and a granular material was supplied through a box suspended above the model in the case of central filling and discharge and through a pipe for eccentric filling and discharge. In experimental analyses the width of the outlet is usually assumed to be 10–50 times the particle diameter. Here the width of the outlet was reduced to 1 cm. This dimension was proper for the amaranthus seed. For the flax-seed it was found that no arches and ratholes form during the flow. The flax seed has its surface plain without any roughnesses, so this property allowed the flow to run without any disturbances. The shape of buckwheat seed remains a pyramid.

The bottom of the supplying box has a sieve and the box was filled with granular material to 2/3 of its height. In another series of experiments, eccentric filling was made where the material was supplied through a pipe placed 1 cm from the left wedge of the model and 1 cm below of the model upper wall. The converging model wall has a shape of a regular triangle with the height 80 cm. The depth of the model is 10 cm with a value of inclination of the walls to the vertical equal 30°. The length of the upper edge of the wall is 102 cm. The model was placed on a stand and a granular material was supplied through a pipe fixed in a box suspended above the model. The box has a volume of 5 l. The pipe was vertically located 5 cm below the upper edge in the model. The converging model was centrally filled with amaranthus seed.

Table 1. Properties of the materials used in the experiments.

Granular material	Wall friction φ_w [°]	Angle of internal friction φ_e [°]	Young modulus [MPa]	Granular material density deposited through a pipe with zero free-fall ρ_b [kg/m^3]
amaranthus	25	28	12.96	832 at 1 kPa 833 at 8 kPa
flax-seed	26	25	6.11	746 at 1 kPa 747 at 8 kPa
buckwheat	28	25	–	669 at 1 kPa 671 at 8 kPa

Moisture of amaranthus seed and flax-seed was also investigated and found to be 10.1% for amaranthus seed and 10.4% for flax-seed. The values of Young modulus of the grains used in the experiments depended on moisture of the grains. More information on physical properties of these and other grains can be found in [25].

Amaranthus grain has a shape of regular round balls of 1 mm diameter, straw-coloured. The surface of the grain is plain. Flax-seed has a shape of flattened rotational ellipse 4 mm × 2 mm, of brown colour and plain, brilliant surface. Buckwheat seed is like a pyramid of total height 2 mm. Its surface is not so brilliant as flax-seed, of a little darker brown colour than the flax-seed.

3. Central flows

3.1. Theory and experiments related to central flows

Many experiments are aimed at investigating the types of flow and shapes of the flowing regions. Behaviour of flowing materials was observed by numerous investigators and some new classifications of funnel flow were introduced, namely semi-mass flow and internal or pipe flow in [51]. The plasticity theory is well established for prediction of strains and stresses in granular materials and can be extended to large strains occuring in flowing materials. It was later found

that the flowing zone predicted by Jenike's radial velocity field appeared far narrower than that observed in actuality [10]. In all experiments researchers considered some flow factors as: hopper geometry, height of packed materials, size of particles, material density, material-wall interface friction of flow patterns [15, 33, 45, 49, 51]. NEDDERMAN stated [32] that, there are no reliable methods for predicting the shape of stagnant zone boundaries. In the case of eccentric filling and discharge the problem is more complicated. CARSON [9] described errors which can cause that silos and bins fail with a frequency which is much higher than that of any other industrial equipment. These errors may be divided into four groups: design errors, construction errors, usage or improper maintenance. Many experimental works have been focused on measurement of flow patterns and different techniques were used there. For example, KVAPIL in [19] used two different colours of the material. The flow was observed through the transparent walls of the model to register flow profiles. Optical techniques are commonly used in the analysis of velocity profiles through the transparent silo walls. The X-ray technique was frequently applied [5, 11] to obtain information from deeper flow layers. Researchers filled the bin in a special way investigating the behaviour of granular materials [49]. Simplified assumptions were also used to analyse the flow. To predict velocities and stagnant boundaries in the flowing material, some theoretical models were used: a rigid perfectly plastic model and a kinematic model [13, 20, 28–30, 49]. Both models assumed the constancy of material density within the bin, i.e., incompressible flow is considered. A "softening" variable-density plastic flow model was introduced by WEIR [52] allowing to consider stresses developing in the funnel-type flow. Evolution of the plug flow zone in time and the position of flow boundaries are the main topics of experimental and theoretical works. In experimental measurements made by WATSON [50] the stagnant zone boundary was shown as a function of time obtained in a hemi-cylindrical bunker. NEDDERMAN in [32] showed the predicted position of the stagnant boundary as a function of time. The kinematic model was used in both investigations and gave an excellent prediction of the development of the stagnant zone boundary in the whole material. Some differences were noticed only close to the orifice. Development of the stagnant boundary in eccentric flows has not been discussed in the literature yet. That is why the researchers have been looking for new possibilities to describe the phenomenon of evolution of the stagnant zone boundary in flowing materials.

3.2. Selected results for the plane model of silo

Figure 2 shows the evolution of the plug flow zone during gravitational discharge in a plane model obtained by PIV measurements. The colour of the contour indicates the magnitude of the velocity. The red colour contours denote the

highest velocity region which developed near the outlet. A funnel of a loose material (like a flame) occured in the central part of the flow after opening the outlet. The region with the highest velocity rapidly reached about 30 cm of the model height. Then the flow was more quiet and the region with the highest velocity reached about 15 cm of the model height. The stagnant zones are indicated by the blue colour of the velocity contour map. The velocity of the flowing material has its maximum on the axis of the model. In the advanced phase of the flow after 52.5 s, "the flame" of the highest velocity again reached the heigher level – about 20 cm.

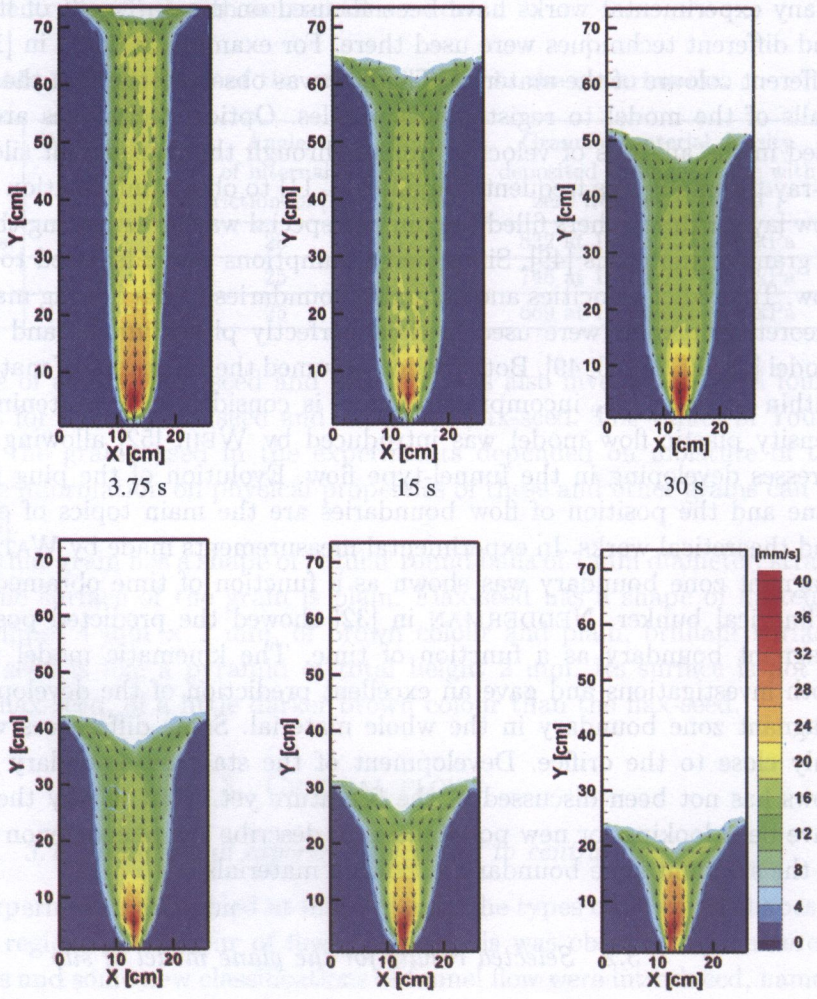

FIG. 2. Velocity fields and velocity magnitude contours in the model with flowing amaranthus after SIELAMOWICZ *et al.* [44].

Figure 3 presents the vector fields and the traces of individual particles (indicated with red colour) obtained for the flowing amaranthus calculated from the velocity field measured in the model. The black vectors denote the flowing region and the lengths of the vectors denote the velocity. In the stagnant zones the points denote vectors of zero value.

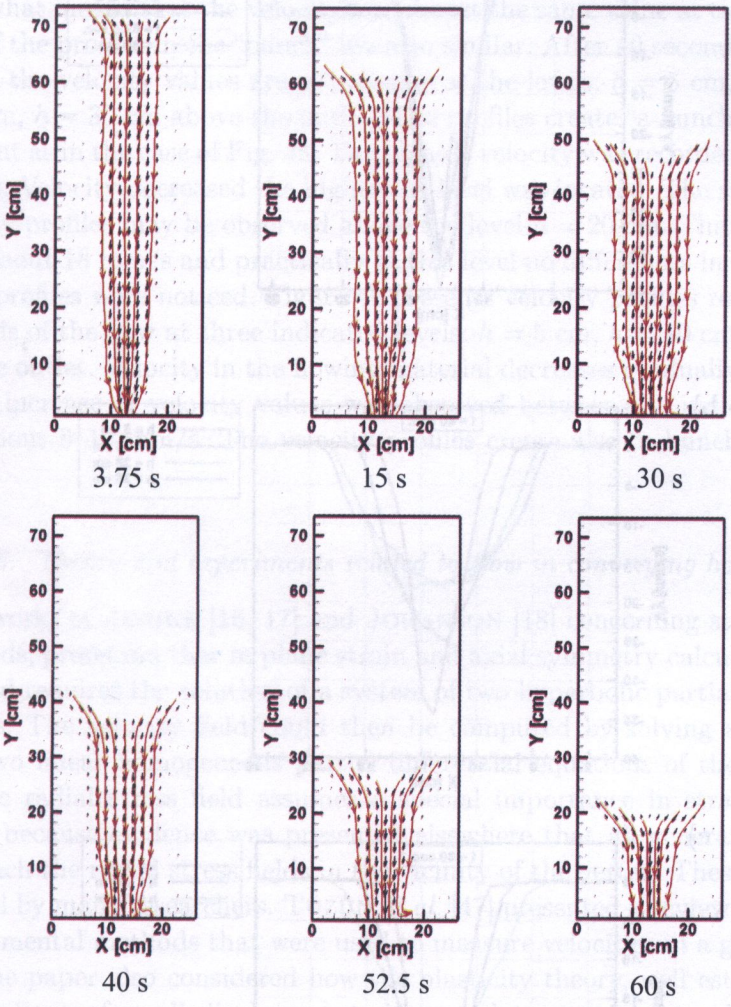

FIG. 3. Traces of individual particles of flowing amaranthus, after SIELAMOWICZ *et al.* [44].

The outer traces are close to the boundary lines of the flowing zone. They are not always vertical or smooth. In [44] some irregular lines were presented. It resulted from the fact that the used seeds were less homogeneous and contained some natural pollutions. The shape of the grains, and the kind of the seed surface influenced their flowing properties. Selected velocity profiles of the flowing amaranthus are shown in Fig. 4. The profiles of the vertical velocity components

across the cavity were obtained at different heights (indicated in the legend) and at different time steps. Here they are presented for 40 s and for 60 s after opening

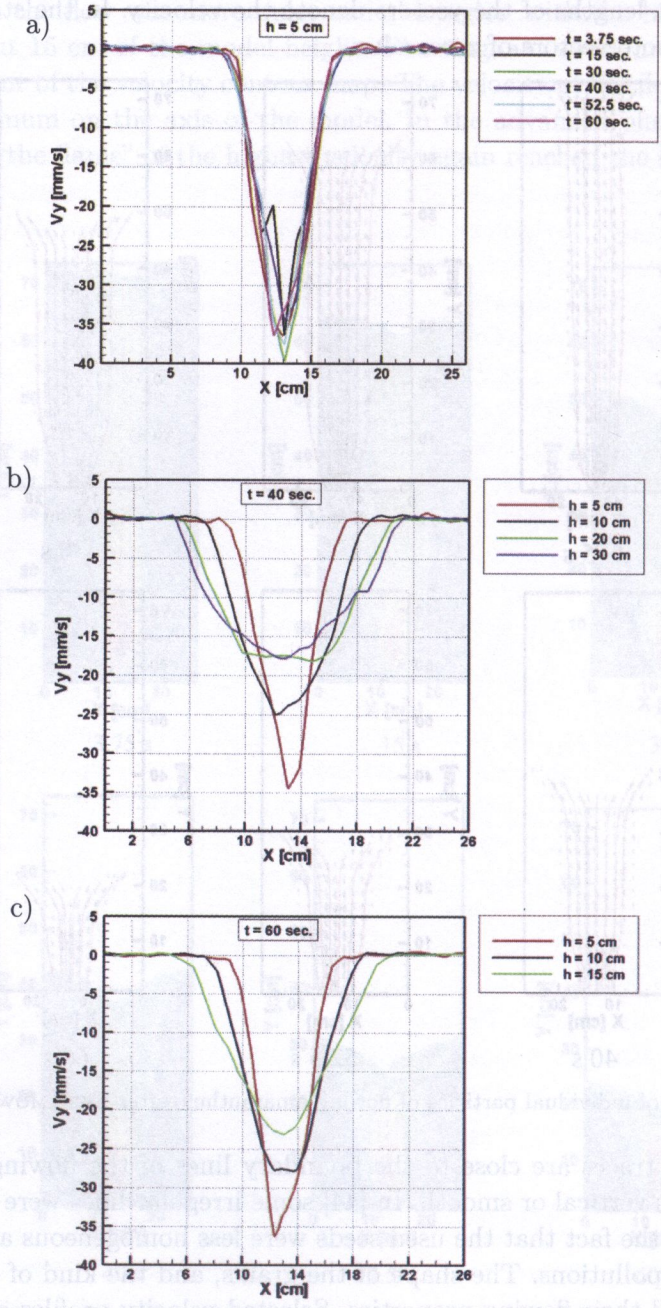

FIG. 4. Velocity profiles for the flow of amaranthus seed.

the outlet. More results obtained for velocity profiles for flowing amaranthus one may find in [44].

In Figure 4a velocity profiles at the level $h = 5$ cm above the outlet were made for the following time steps: $t = 3.75$ s, $t = 15$ s, $t = 30$ s, $t = 40$ s, $t = 52.5$ s, $t = 60$ s. One may observe that the velocities create "a bunch" of profiles what means that the velocity has almost the same value at this level. The shapes of the profiles in the "bunch" are also similar. After 40 seconds of the flow (Fig. 4b) the velocity values are not similar at the levels: $h = 5$ cm, $h = 10$ cm, $h = 20$ cm, $h = 30$ cm above the outlet. The profiles create "a bunch" but not so convergent as in the case of Fig. 4a. The highest velocity was recorded at the level $h = 5$ cm. Velocity decreased the higher the level was located. The similar shape of velocity profiles may be observed above the level $h = 20$ cm. The velocity has a value about 18 mm/s and practically at this level no differences in the shape of velocity profiles were noticed. Figure 4c presents velocity profiles recorded after 60 seconds of the flow at three indicated levels: $h = 5$ cm, $h = 10$ cm, $h = 15$ cm above the outlet. Velocity in the flowing material decreases gradually up. Rather constant increase of velocity values was observed between the indicated levels. It was about 8–10 mm/s. The velocity profiles create also "a bunch" of similar shapes.

3.3. Theory and experiments related to flow in converging hoppers

The works of JENIKE [16, 17] and JOHANSON [18] concerning stress and velocity fields, presented that in plane strain and axial symmetry calculation of the stress field requires the solution of a system of two hyperbolic partial differential equations. The velocity field could then be computed by solving another system of two linear homogeneous partial differential equations of the hyperbolic type. The radial stress field assumes a special importance in straight conical channels because evidence was presented elsewhere that all general fields tend to approach the radial stress fields in the vicinity of the vertex. These ideas were developed by many researchers. TÜZÜN *et al.* [47] presented a review article with all experimental methods that were used to measure velocities in a granular material. The paper also considered how the plasticity theory, well established for the predictions of small displacements in granular materials, can be extended to the effectively infinite strains found in flowing systems. This was compared with alternative methods of predicting velocity distributions based on the kinematic hypothesis without reference to the stress state, proposed by LITWINISZYN [20] and developed by MULLINS [28, 29]. The details of experimental measurements of velocity distributions and comparisons with the theoretical predictions were presented. In the review article, TÜZÜN *et al.* [47] discussed both two- and three-dimensional flows, and both wedge-shaped and conical hoppers. Later,

the measurement techniques of flows and theoretical approaches were developed. However, other authors reported the existence of discontinuities in velocity fields. MICHAŁOWSKI [22] presented some experimental results of investigation of flow patterns in a plane, wedge-shaped hopper, and also an approach to a theoretical description of discharge. A non-steady discontinuous velocity field was measured using a stereophotographic technique. A series of X-ray pictures and ultrasonic measurements presented the density distribution in the flowing material. The velocity field was restricted to the advanced stage of flow, which was treated as a pseudo-steady process. A theoretical description of the kinematics of the advanced phase of the flow, based on the plane plastic flow theory of an incompressible material, coupled with the radial stress field described the actual velocity field, particularly in hoppers with smooth walls. A similar strategy of solving kinematics in hoppers, was also proposed by PARISEAU [35]. The results presented by MICHAŁOWSKI [22] were similar to those obtained by DRESCHER *et al.* [11]. Stress and velocity fields in two- and three-dimensional hoppers, were also considered by PITMAN [36] in the steady-state flow of an incompressible, cohesionless granular material. A numerical method for solving the equations governing the flow of a granular material was presented by PITMAN [36] and the solution was extended for application to three-dimensional hoppers. POLDERMAN *et al.* [37] proposed a calculation method which gave a good prediction for the velocity distribution in mass flow hoppers (wedge-shaped and conical). The method was based on the classical plasticity theory. The results given in [36] supported the assumptions about the distribution of the stress components made by Walker's differential slice model [48]. The initial stage of discharge in plane asymmetrical converging hoppers was also further investigated by MICHAŁOWSKI [23]. The determination of the propagation of the rapture bands and density variation were shown and theoretical considerations were based on the theory of plastic flow. The stress distribution and the boundary problems for velocities using the associated and non-associated flow rules were solved. NEDDERMAN in [31] presented a new technique for measuring the velocity distributions in conical hoppers. Marker particles were released in the already-flowing material. The velocity distributions were deduced from the measured times of passage. A minor effect of the size and density of the marker particles was shown and the velocity of these particles adequately represent the velocity of granular material. The theoretical predictions given by JENIKE [17], and among others by MRÓZ and SZYMAŃSKI [27], were reviewed and two original modifications were presented. The method introduced by NEDDERMAN [31] showed that the marker particles move with the same velocity as the surrounding material and this assumption was confirmed by the experimental results. The only small dependence of the time of passage on the size and density of the marker particles showed that there was no need to match the marker and bulk particles closely. By integrating the velocity profiles,

the flow rate was calculated. It proved a good agreement with the measured values independently, giving confidence to the accuracy of the method. Calculations in wedge-shaped hoppers do not give a satisfactory approach to the radial stress and velocity fields. Calculations in conical geometries appeared successful only for either materials of unrealistic angles of friction, or for circumstances in which the stresses at the top surface were close to those predicted by the radial, stress field. CLEAVER and NEDDERMAN'S [10] experiments showed that the velocities in the lower half of a conical hopper are radial, with magnitudes similar to those predicted from the radial velocity field. MOREEA and NEDDERMAN [32] used the method of characteristics to predict the exact stress and velocity fields in an incompressible, cohesionless Coulomb material discharging from a conical hopper for a great variety of boundary conditions imposed on the upper surface. They found that in all cases, stress and velocity tend to the radial stress and velocity fields, and that convergence was achieved about half-way down the hopper. The velocity fields show the regions of more or less constant velocity separated by velocity characteristics. This statement made by MOREEA and NEDDERMAN [26] justified the assumption in Drescher's method of predicting velocity distributions [12]. WATSON and ROTTER [51] used the finite element analysis to calculate the steady-state velocity in a cohesionless granular material discharging from a planar flat-bottomed silo. The relationship between the horizontal velocity and the horizontal gradient of the vertical velocity was the basic assumption in the analysis. Deformation rate, velocity fields, and stress distributions were calculated without the need of re-meshing the FE-grid in a model of converging silo by BÖHRNSEN *et al.* [7] who used the finite element method based on the Euler's reference frame. The flow profiles were investigated and the stress evolution was recorded, e.g., a stress switch moving from the outlet to the transition from the hopper to shaft.

3.4. Selected results obtained for the converging model

The model was filled with 55 cm-high of amaranthus and with 56 cm-high of flax seed. The discharge rate was measured by a scales. The discharge time for amaranthus was found to be 234 s and for flax-seed 170 s. It was found that the mass discharge rate was not uniform during the whole time of the flow, but measured at a time interval every 30 s, decreasing as the material flowed (Fig. 5).

The discharge rate for amaranthus seed was found to be constant till 150 s, measured as 2.23 kg. After this time, the discharge rate rapidly decreased to the value of 1.75 kg (after 180 s of the flow) and 1.35 kg (after 210 s of the flow). A similar situation was observed during the flow of flax-seed. It results from the fact that in the last phase of the flow the material in the model had considerably lower density than in the initial phase of the flow. Both materials,

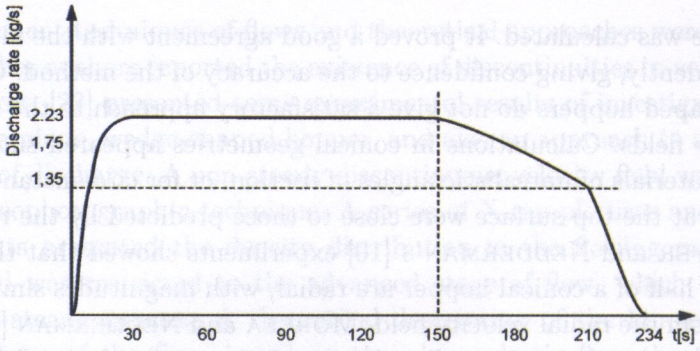

FIG. 5. Discharge rate for amaranthus seeds.

after filling, formed the upper free surface of a constant slope at an angle equal to the material's angle of repose. With progressing discharge the upper surface lowers. The evolution of the upper surface for flowing amaranthus seed is shown in Fig. 6. Figure 6 also presents vector fields in the material. It is seen that the width of the plug flow zone increases rapidly. The boundaries of the flow region away from the outlet are vertical. In the vicinity of the outlet the boundaries of the flow region are slightly curved and the velocity vectors are directed towards the outlet. The vectors located near the upper surface are directed towards the flow region and they indicate the direction of the flow in this region. DPIV images

a)

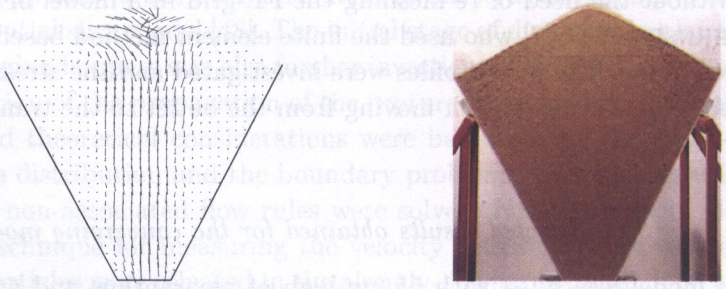

b)

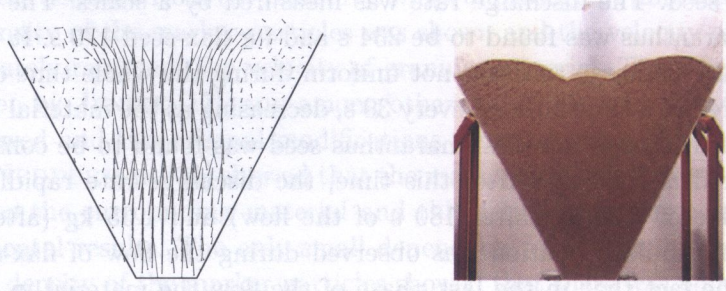

FIG. 6 a, b

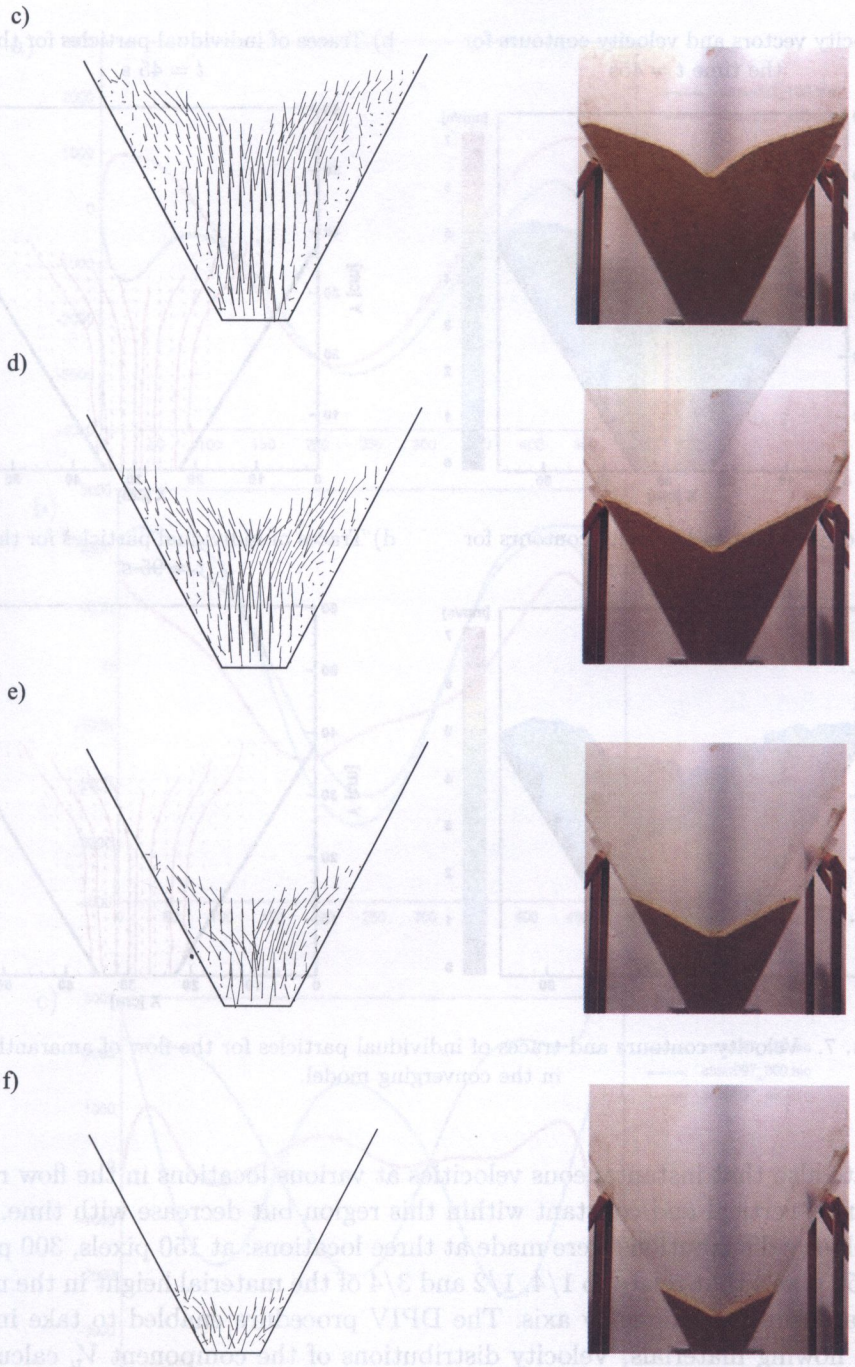

FIG. 6. Consecutive stages of the flow in the converging model and the vector fields related to the flow; a) Flow after 5 s. b) Flow after 45 s. c) Flow after 95 s. d) Flow after 145 s. e) Flow after 175 s. f) Flow after 205 s.

a) Velocity vectors and velocity contours for the time $t = 45$s

b) Traces of individual particles for the time $t = 45$ s

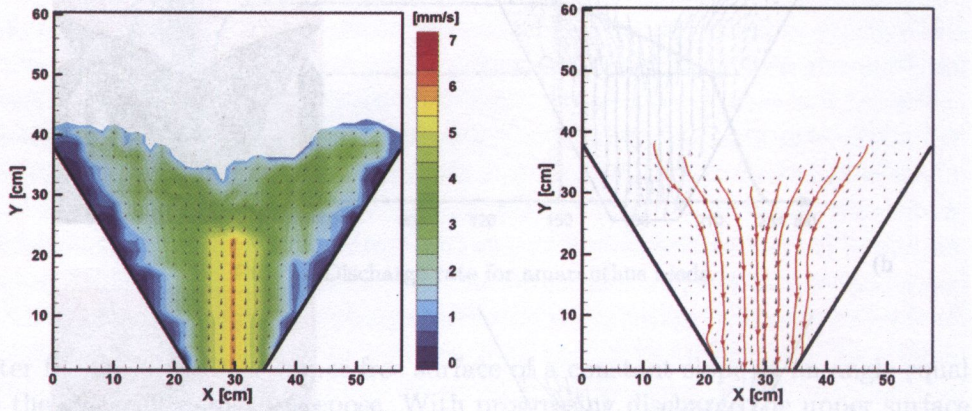

c) Velocity vectors and velocity contours for the time $t = 95$ s

d) Traces of individual particles for the time $t = 95$ s

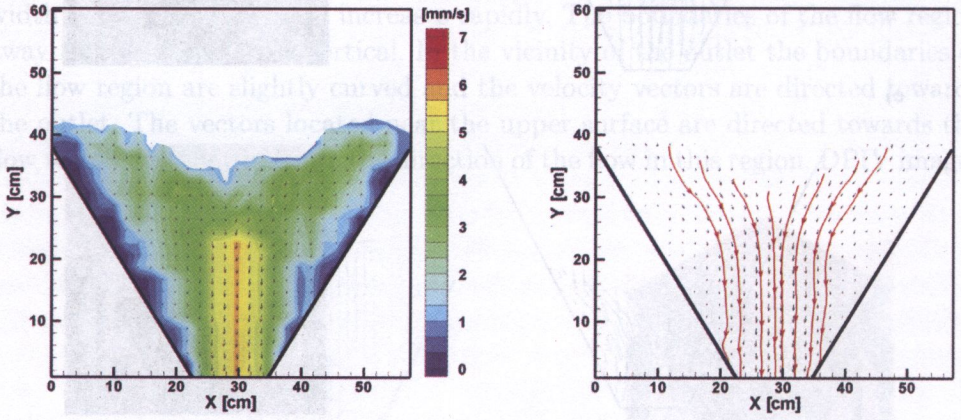

FIG. 7. Velocity contours and traces of individual particles for the flow of amaranthus in the converging model.

indicate also that instantaneous velocities at various locations in the flow region appear as vertical and constant within this region but decrease with time.

Velocity distributions were made at three locations: at 150 pixels, 300 pixels, and 450 pixels that relate to 1/4, 1/2 and 3/4 of the material height in the model calculated in the symmetry axis. The DPIV procedure enabled to take images of the flowing materials. Velocity distributions of the component V_y calculated for the selected images at the above mentioned locations are presented below. In the upper right corner the number of the image and the value of the location are indicated. Figure 8 presents velocity profiles for the flow of amaranthus. Some

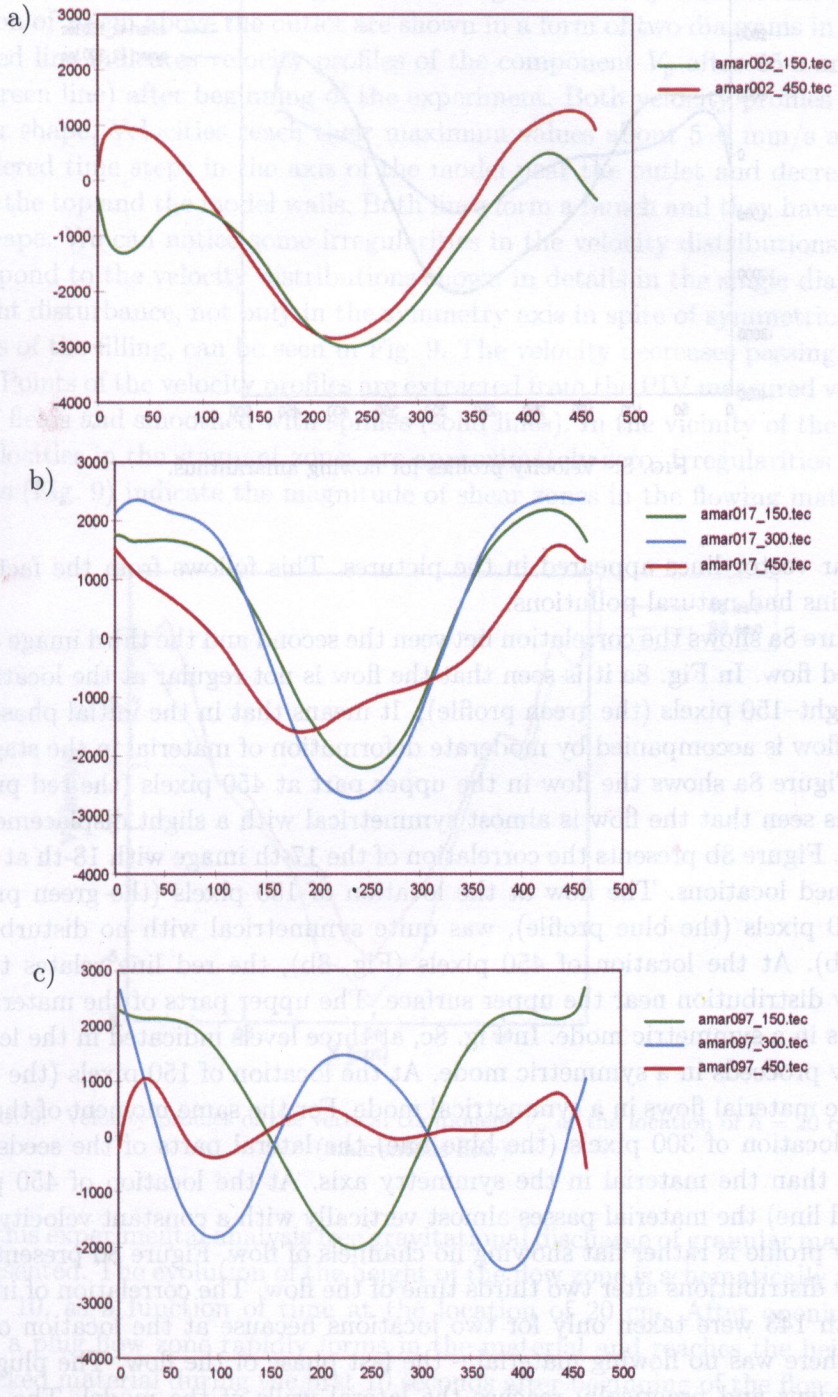
a)
3000
2000
1000
0
-1000
-2000
-3000
-4000
0 50 100 150 200 250 300 350 400 450 500
amar002_150.tec
amar002_450.tec
b)
3000
2000
1000
0
-1000
-2000
-3000
-4000
0 50 100 150 200 250 300 350 400 450 500
amar017_150.tec
amar017_300.tec
amar017_450.tec
c)
3000
2000
1000
0
-1000
-2000
-3000
-4000
0 50 100 150 200 250 300 350 400 450 500
amar097_150.tec
amar097_300.tec
amar097_450.tec

[FIG. 8 a, b, c]

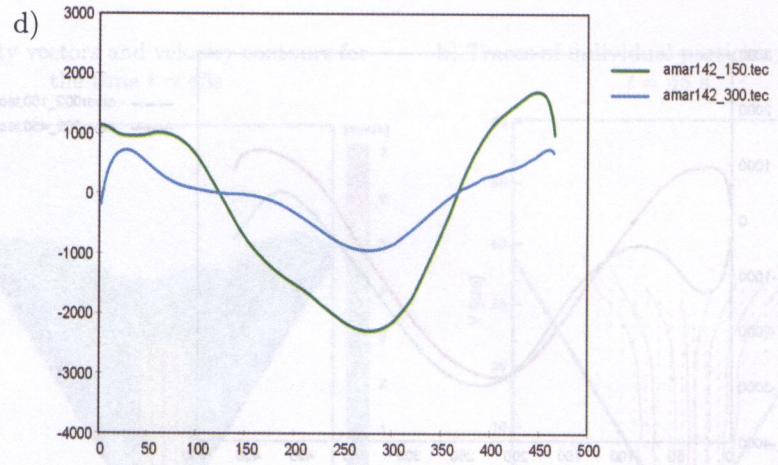

FIG. 8. Velocity profiles for flowing amaranthus.

irregular vector lines appeared in the pictures. This follows from the fact that the grains had natural pollutions.

Figure 8a shows the correlation between the second and the third image of the recorded flow. In Fig. 8a it is seen that the flow is not regular at the location of 1/4 height–150 pixels (the green profile),. It means that in the initial phase, the funnel flow is accompanied by moderate deformation of material in the stagnant zone. Figure 8a shows the flow in the upper part at 450 pixels (the red profile) and it is seen that the flow is almost symmetrical with a slight displacement to the left. Figure 8b presents the correlation of the 17-th image with 18-th at three mentioned locations. The flow at the location of 150 pixels (the green profile) and 300 pixels (the blue profile), was quite symmetrical with no disturbances (Fig. 8b). At the location of 450 pixels (Fig. 8b), the red line relates to the velocity distribution near the upper surface. The upper parts of the material do not pass in a symmetric mode. In Fig. 8c, at three levels indicated in the legend, the flow proceeds in a symmetric mode. At the location of 150 pixels (the green line) the material flows in a symmetrical mode. For the same moment of the flow at the location of 300 pixels (the blue line) the lateral parts of the seeds pass quicker than the material in the symmetry axis. At the location of 450 pixels (the red line) the material passes almost vertically with a constant velocity. The velocity profile is rather flat showing no channels of flow. Figure 8d presents the velocity distributions after two thirds time of the flow. The correlation of images 142 with 143 were taken only for two locations because at the location of 450 pixels there was no flowing material – the last phase of the flow. The plug flow zone widens and practically reaches the lateral walls of the model. The green and the blue line relate to the locations of 150 and 300 pixels, respectively.

The results presented in Fig. 8 concerning the velocity distributions at the location of 20 cm above the outlet are shown in a form of two diagrams in Fig. 9. The red line indicates velocity profiles of the component V_y after 45 s and 90 s (the green line) after beginning of the experiment. Both velocity profiles have a similar shape. Velocities reach their maximum values about 5–6 mm/s at both considered time steps in the axis of the model near the outlet and decrease towards the top and the model walls. Both lines form a bunch and they have a similar shape. We can notice some irregularities in the velocity distributions. They correspond to the velocity distributions shown in details in the single diagrams. A slight disturbance, not only in the symmetry axis in spite of symmetrical conditions of the filling, can be seen in Fig. 9. The velocity decreases passing to the walls. Points of the velocity profiles are extracted from the PIV measured velocity vector fields and smoothed with splines (solid lines). In the vicinity of the outlet the velocities in the stagnant zones are approximately zero. Irregularities on the profiles (Fig. 9) indicate the magnitude of shear zones in the flowing material.

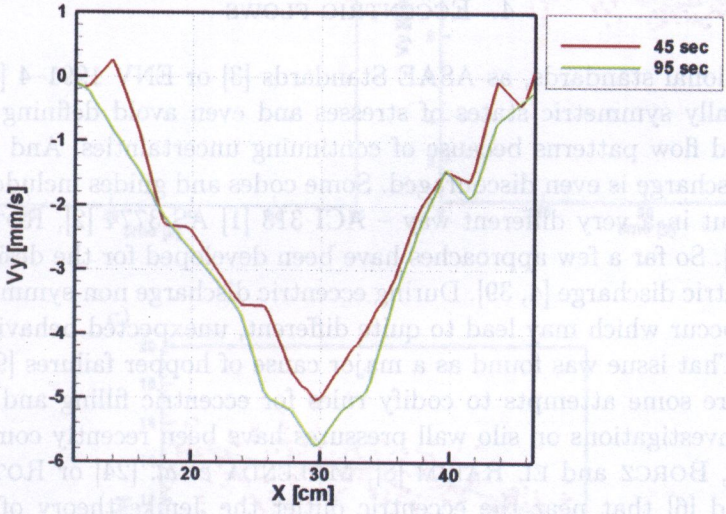

FIG. 9. Velocity profiles of the vertical component V_y at the location of $h = 20$ cm (amaranthus flow).

In this experimental analysis free gravitational discharge of granular materials are presented. The evolution of the height of the flow zone is schematically shown in Fig. 10, as a function of time at the location of 20 cm. After opening the outlet, a plug flow zone rapidly forms in the material and reaches the height of the packed material during the first 10 seconds after beginning of the flow. From the beginning of the flow till about 160 s of the flow, the evolution of the plug flow zone is represented by a slightly concave line.

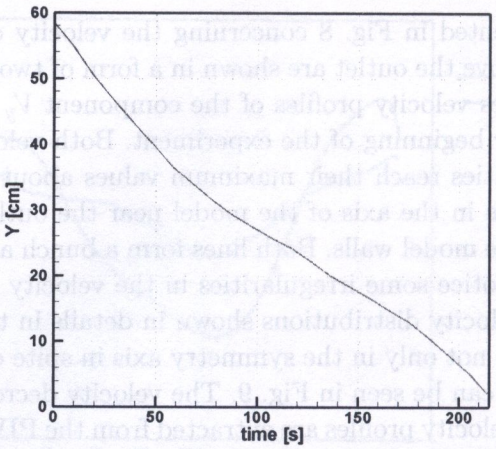

FIG. 10. Evolution of the height of the flow zone measured in the symmetry axis (amaranthus flow).

4. ECCENTRIC FLOWS

International standards, as ASAE Standards [3] or ENV 1991–4 [14], relate only to axially symmetric states of stresses and even avoid defining discharge pressure and flow patterns because of continuing uncertainties. And the use of eccentric discharge is even discouraged. Some codes and guides include eccentric discharge but in a very different way – ACI 313 [1] AS 3774 [2], ROTTER [40], JENIKE [18]. So far a few approaches have been developed for the design of bins under eccentric discharge [4, 39]. During eccentric discharge non-symmetrical bin wall loads occur which may lead to quite different, unexpected behaviour of the structure. That issue was found as a major cause of hopper failures [9].

There are some attempts to codify rules for eccentric filling and discharge and some investigations on silo wall pressures have been recently completed by BLIGHT [6], BORCZ and EL RAHIM [8], MOLENDA *et al.* [24] or ROTTER [39]. Blight found [6] that near the eccentric outlet the Jenike theory of pressures is also valid for the case of eccentric emptying. AYUGA *et al.* [4] investigated pressure distribution in discharge process in a silo with central and eccentric outlets and described the influence of outlet eccentricity. MOLENDA *et al.* [24] investigated bin loads induced by eccentric filling and discharge of grain. It was found that eccentric discharge induced dynamic moments much higher than static moments on the bin wall.

In this experimental work in the case of eccentric flow, the plane model was filled with flax-seed in asymmetrical way as it was described above. Figsures 11 a, b, c present vertical velocity variations in time in the model for the three cases investigated here.

In the case of Figs. 11 a, c the velocity distributions differ rather slightly. The values of velocities are higher in the case of Fig. 11 a. But Fig. 11 b shows the velocity distribution for the central discharge. The flow of the material tends to become symmetrical in spite of the way of filling and tries to form a symmetric flow. Flow patterns obtained in the case of non-symmetrical filling and discharge are different than in the case of central flows. There are quite different load distributions, velocity distributions, velocity profiles if the outlet is placed not in the symmetry axis of the bin. In these cases we cannot predict the inherent behaviour of the material.

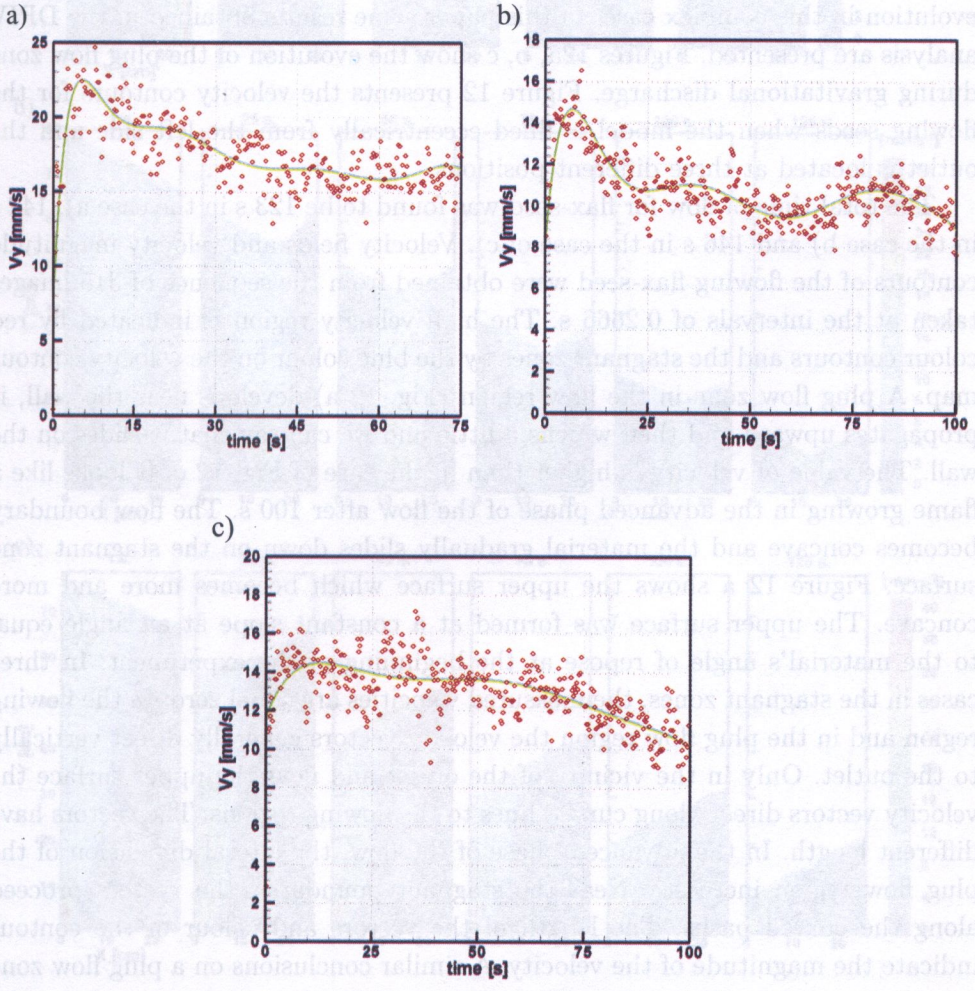

FIG. 11. Vertical velocity distributions for flax seed in the model with eccentric filling located 1 cm from the left edge of the model and discharge from a) the right, b) in the central line, c) the left.

4.1. Velocity profiles

In the literature we can find few experimental measurements of the stagnant zone boundaries in bins/hoppers with eccentric filling and discharge. More approaches concern central filling and discharge in silos. WATSON and NEDDERMAN presented [32, 50] the development of stagnant zone boundaries obtained from the predictions and experiments in a symmetrical case. Their results are compared in SIELAMOWICZ *et al.* [44] to the experimental results obtained by DPIV technique. In fact there are only few studies in the literature so it seems to be a valuable task to undertake this challenge and try to investigate flow evolution in this complex case. In this paper some results obtained in the DPIV analysis are presented. Figures 12a, b, c show the evolution of the plug flow zone during gravitational discharge. Figure 12 presents the velocity contours for the flowing seeds when the model is filled eccentrically from the left side and the outlet is located at three different positions.

The total time of flow for flax-seed was found to be 123 s in the case a), 142 s in the case b) and 146 s in the case of c). Velocity fields and velocity magnitude contours of the flowing flax-seed were obtained from the sequence of 315 images taken at the intervals of 0.2666 s. The high velocity region is indicated by red colour contours and the stagnant zones by the blue colour on the velocity contour map. A plug flow zone in the flow region (Fig. 12 a) develops near the wall, it propagates upward and then widens a little and we can say that it slides on the wall. The value of velocity is higher than in the case of Fig. 12 c. It looks like a flame growing in the advanced phase of the flow after 100 s. The flow boundary becomes concave and the material gradually slides down on the stagnant zone surface. Figure 12 a shows the upper surface which becomes more and more concave. The upper surface was formed at a constant slope at an angle equal to the material's angle of repose at the beginning of the experiment. In three cases in the stagnant zones, the measured velocities are equal zero. In the flowing region and in the plug flow region the velocity vectors generally direct vertically to the outlet. Only in the vicinity of the outlet and near the upper surface the velocity vectors direct along curved lines to the flowing regions. The vectors have different length. In the advanced phase of the flow, the lateral dimension of the plug flow region increases. Near the stagnant boundaries the vectors proceed along the curved paths. The length of the vectors and colour of the contour indicate the magnitude of the velocity. A similar conclusions on a plug flow zone can be drawn from Figs. 12 c. The outlet is located at the same side as the filling was made. And now we observe a similar forming of the plug flow but the velocity in the flowing region is a little lower than in Figs. 12 a that is indicated

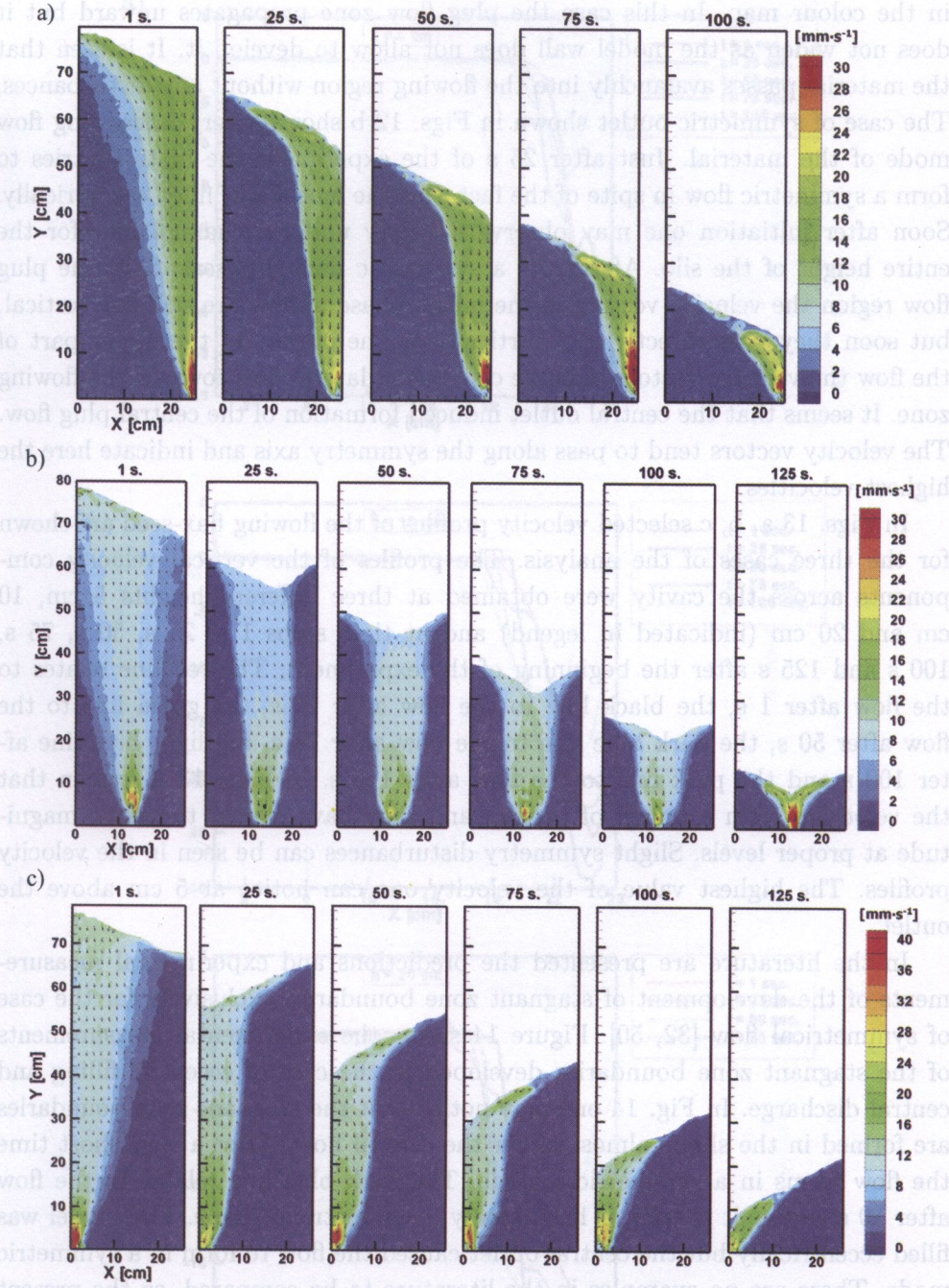

FIG. 12. Velocity contours for the eccentric filling in the left part of the model and a) discharge on the right, b) central discharge, c) discharge in the left part of the model (after SIELAMOWICZ *et al.* [42]).

in the colour map. In this case the plug flow zone propagates upward but it does not widen as the model wall does not allow to develop it. It is seen that the material passes avalanchly into the flowing region without any disturbances. The case of symmetric outlet shown in Figs. 12 b shows a very interesting flow mode of the material. Just after 25 s of the experiment the material tries to form a symmetric flow in spite of the fact that the model was filled eccentrically. Soon after initiation one may observe a nearly uniform channel flow for the entire height of the silo. After 25 s a symmetric flow is observed. In the plug flow region the velocity vectors in the initial phase of flow are still not vertical, but soon they pass directly and vertically to the outlet. In the upper part of the flow the velocity vectors indicate converging lateral flow towards the flowing zone. It seems that the central outlet induced formation of the central plug flow. The velocity vectors tend to pass along the symmetry axis and indicate here the highest velocities.

In Figs. 13 a, b, c selected velocity profiles of the flowing flax-seed are shown for the three cases of the analysis. The profiles of the vertical velocity components across the cavity were obtained at three different heights 5 cm, 10 cm and 20 cm (indicated in legend) and at time steps 1 s, 25 s, 50 s, 75 s, 100 s and 125 s after the beginning of the experiment. The red line relates to the flow after 1 s, the black line to the flow after 25 s, the green line to the flow after 50 s, the dark blue line to the flow after 75 s, the light blue line after 100 s and the pink line to the flow after 125 s. In Figs. 13 it is seen that the velocities form a bunch of profiles and they have almost the same magnitude at proper levels. Slight symmetry disturbances can be seen in the velocity profiles. The highest value of the velocity one can notice at 5 cm above the outlet.

In the literature are presented the predictions and experimental measurements of the development of stagnant zone boundaries exclusively for the case of symmetrical flow [32, 50]. Figure 14 shows the experimental measurements of the stagnant zone boundaries developed in the case of eccentric filling and central discharge. In Fig. 14 one may notice that the stagnant zone boundaries are formed in the shape almost as for the central flow. After a very short time the flow forms in a symmetrical mode. The dark blue line relates to the flow after 10 s and as it is seen, it has already a symmetrical shape. The model was filled eccentrically but the central outlet caused the flow to form in a symmetric mode. There are no examples in the literature to be compared, so the present study provides interesting information on the shape of boundaries between the flow and stagnant zones.

a)

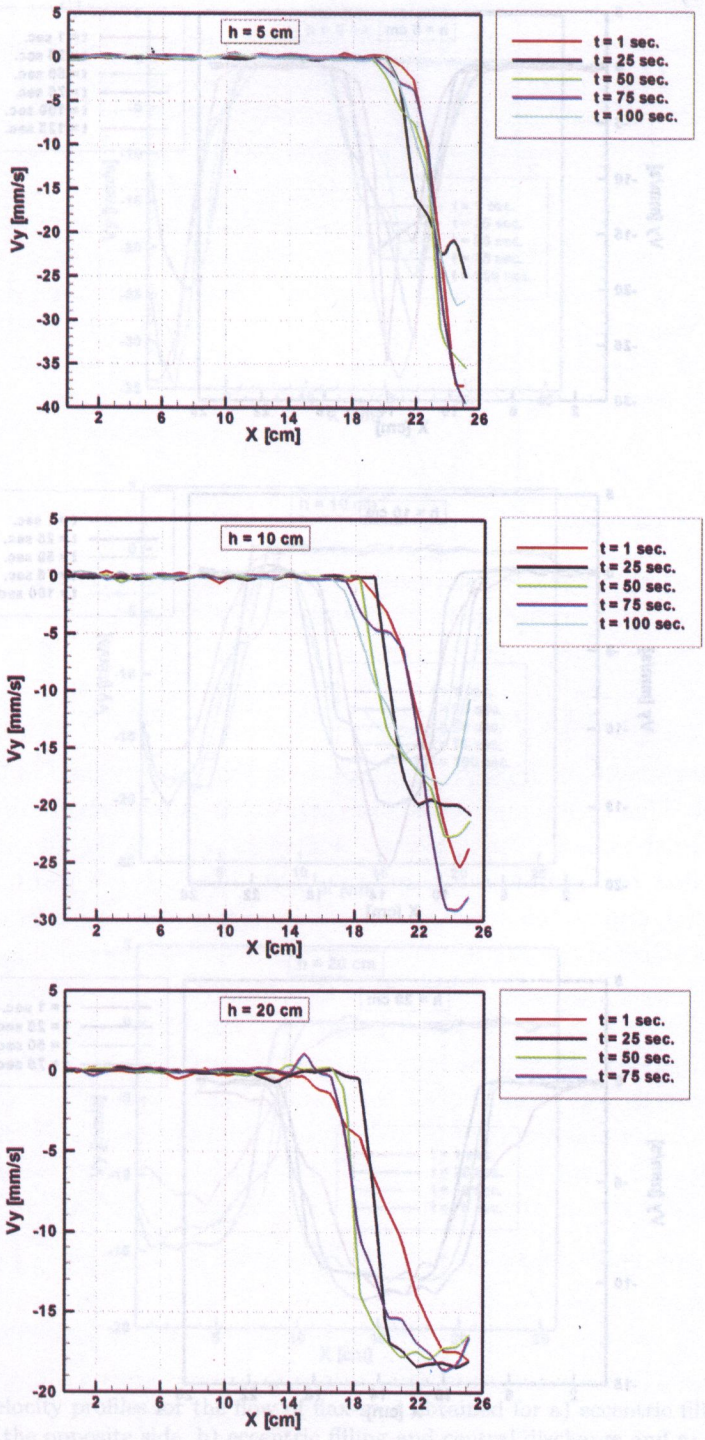
h = 5 cm
t = 1 sec.
t = 25 sec.
t = 50 sec.
t = 75 sec.
t = 100 sec.
Vy [mm/s]
X [cm]
h = 10 cm
t = 1 sec.
t = 25 sec.
t = 50 sec.
t = 75 sec.
t = 100 sec.
Vy [mm/s]
X [cm]
h = 20 cm
t = 1 sec.
t = 25 sec.
t = 50 sec.
t = 75 sec.
Vy [mm/s]
X [cm]

[FIG. 13 a]

b)

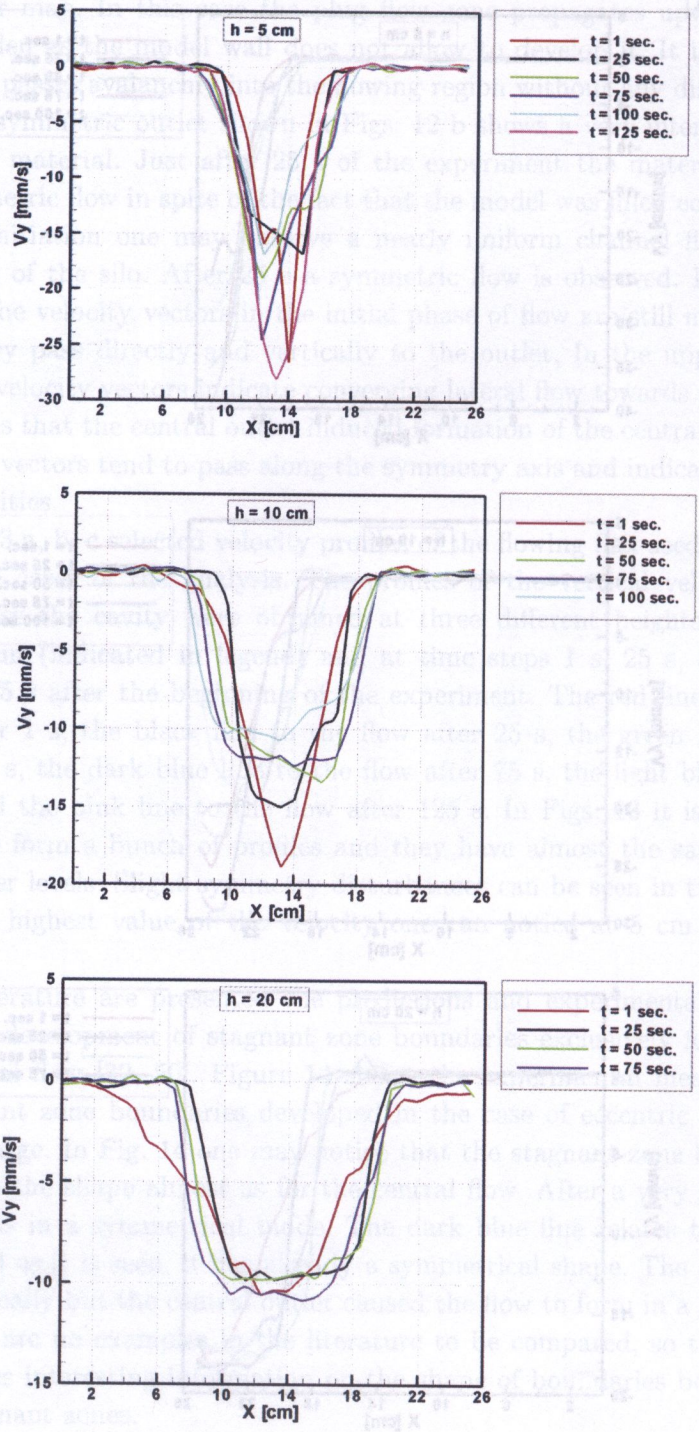
h = 5 cm
t = 1 sec.
t = 25 sec.
t = 50 sec.
t = 75 sec.
t = 100 sec.
t = 125 sec.
Vy [mm/s]
X [cm]
h = 10 cm
t = 1 sec.
t = 25 sec.
t = 50 sec.
t = 75 sec.
t = 100 sec.
Vy [mm/s]
X [cm]
h = 20 cm
t = 1 sec.
t = 25 sec.
t = 50 sec.
t = 75 sec.
Vy [mm/s]
X [cm]

[FIG. 13 b]

c)

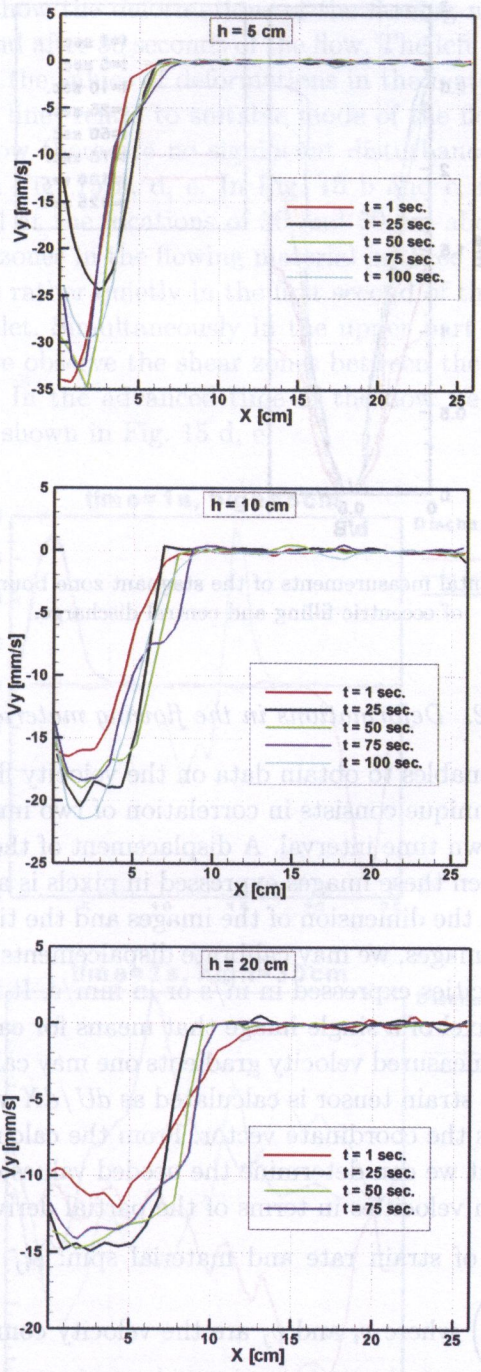

FIG. 13. Velocity profiles for the flow of flax-seed obtained for a) eccentric filling and discharge on the opposite side, b) eccentric filling and central discharge and c) eccentric filling and discharge but on the same side of the model.

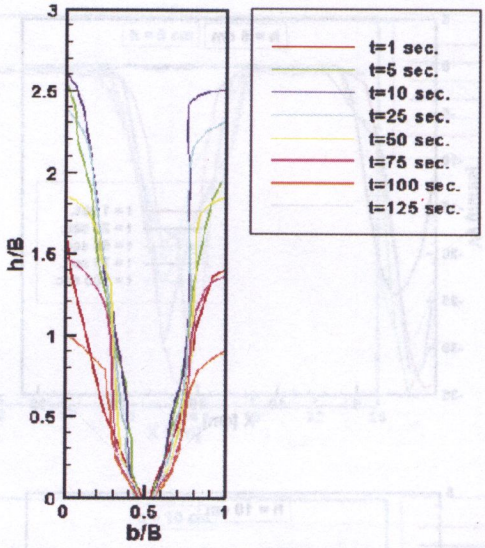

FIG. 14. Experimental measurements of the stagnant zone boundaries in the case of eccentric filling and central discharge.

4.2. Deformations in the flowing material

DPIV technique enables to obtain data on the velocity field in the whole analyzed area. This technique consists in correlation of two images of the recorded flow taken in the known time interval. A displacement of the elements of the investigated flow between these images expressed in pixels is a result of this correlation. Having known the dimension of the images and the time interval between the two investigated images, we may calibrate dispalcements obtained in the correlation into the velocities expressed in m/s or in mm/s. It is possible to obtain these data for each pixel of a single image that means for each point of the analyzed flow. From the measured velocity gradients one may calculate strains in the flowing material. The strain tensor is calculated as dU/dX where U is a velocity vector and X denotes the coordinate vector. From the calculated flow velocities obtained in each point we can determine the needed values of velocity gradients or the values of strain velocities in terms of the partial derivatives. The relation dU/dX is the value of strain rate and material spin: $\dot{\varepsilon}_{ij} = \frac{1}{2}\left(\frac{\partial v_i}{\partial x_j} + \frac{\partial v_j}{\partial x_i}\right)$, $\dot{\omega}_{ij} = \frac{1}{2}\left(\frac{\partial v_i}{\partial x_j} - \frac{\partial v_j}{\partial x_i}\right)$ where v_i and v_j are the velocity components. Measuring the displacement field $u_i(x, y)$, the strain component can be calculated, namely the Green strain tensor $E_{ij} = \frac{1}{2}\left(\frac{\partial u_i}{\partial x_j} + \frac{\partial u_j}{\partial x_i} + \frac{\partial u_k}{\partial x_i}\frac{\partial u_k}{\partial x_i}\right)$.

Figures 15 a–e show the deformations of the flowing material after the first second of the flow and after 50 seconds of the flow. The left axis is denoted by 1/s and the scale shows the values of deformations in the material. The legend (the blue, red and green line) relate to suitable mode of the flow. For the presented time steps of the flow there are no significant disturbances in the flow for the case of discharge in Fig. 15 a, d, e. In Fig. 15 b and c, in the upper parts of the flowing material at the locations of 30 and 50 cm above the outlet we can recognize the shear zones in the flowing material in three analyzed modes of the flow. The flow runs rather quietly in the first second of the flow at the location 5 cm above the outlet. Simultaneously in the upper part the material flows in a such mode that we observe the shear zones between the flowing material and the stagnant zones. In the advanced time of the flow we observe rather quiet flow mode and it is shown in Fig. 15 d, e.

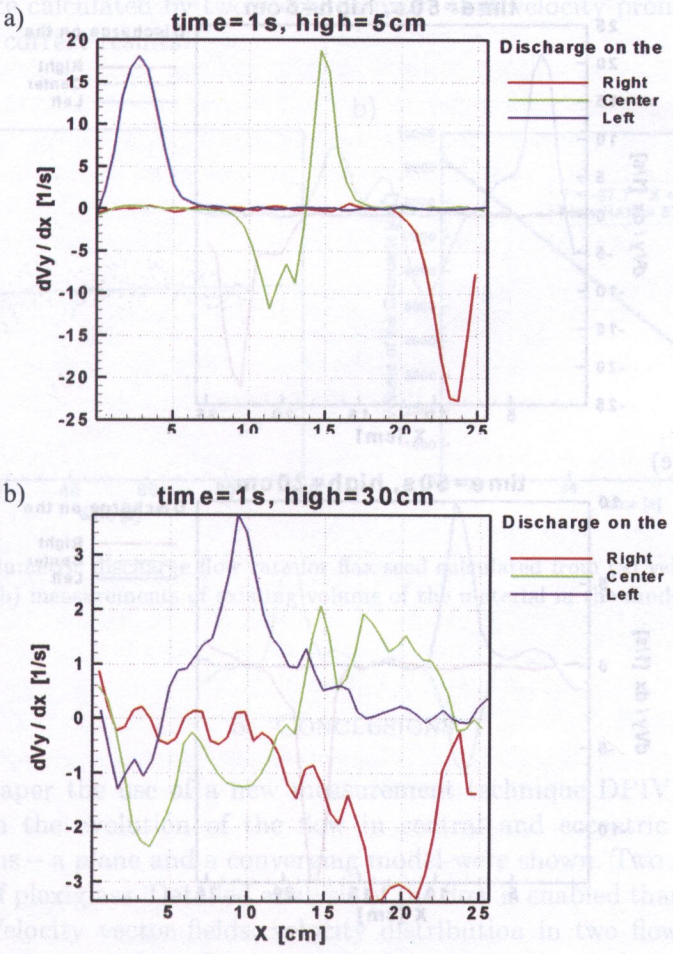

FIG.15a, b

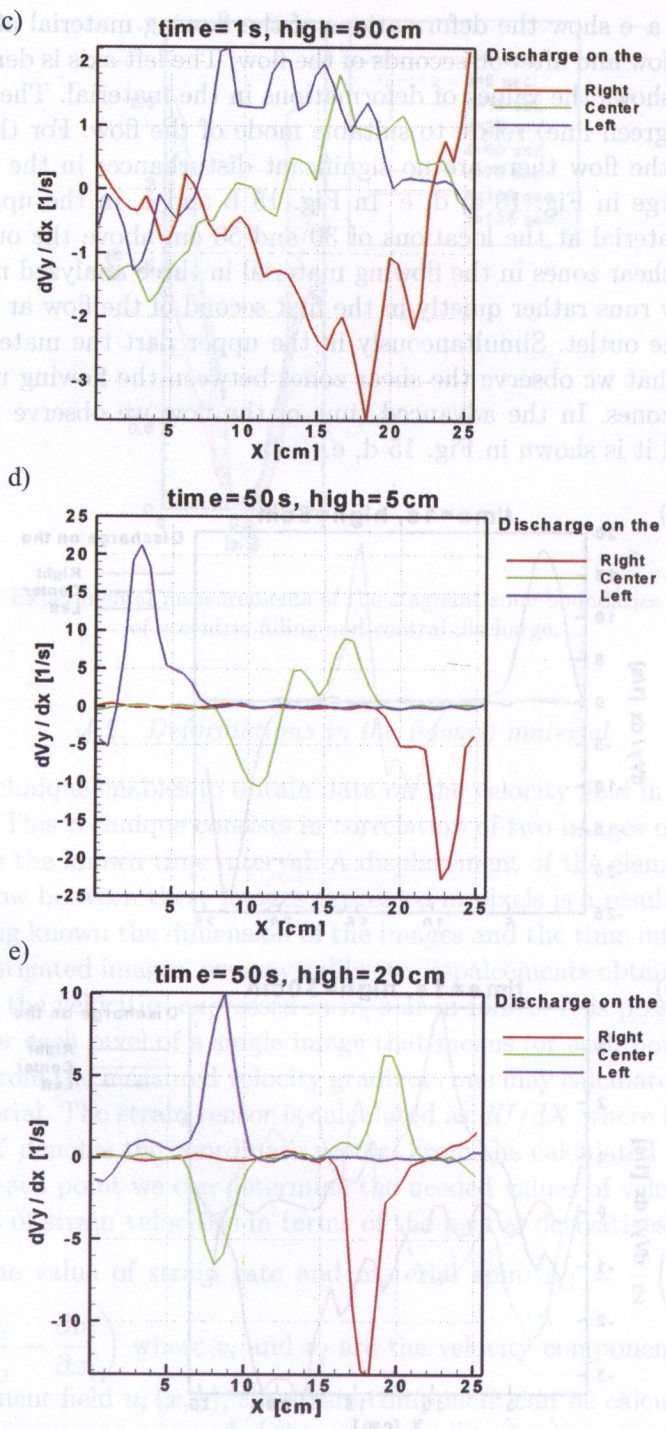

FIG. 15. Deformations in the flowing flax seed in the three cases of eccentric discharge.

4.3. Discharge flow rate calculated from PIV

In Fig. 16 the discharge flow rate calculated by two methods is presented. Each point corresponds to one rate value. The points in Fig. 16 a were calculated from the velocity profiles and then smoothed to a line which represents the discharge volume rate. So, at first the velocity field was obtained and then at the level 20 cm above the outlet the velocity profiles were depicted. These velocity profiles were integrated and the flow rate at each second was calculated. In the case of the results presented in Fig. 16 a one should state that the result is burdened by an error which results from the fact that velocity profiles obtained in computer calculations were in another step of data processing. Already at this step of calculations some errors in accuracy were introduced. Figure 16 b presents the points which were smoothed by a line. The discharge rate was calculated for each picture obtained from PIV. One may state that two obtained results of the discharge rate calculated by two methods prove that velocity profiles calculated by PIV give correct results.

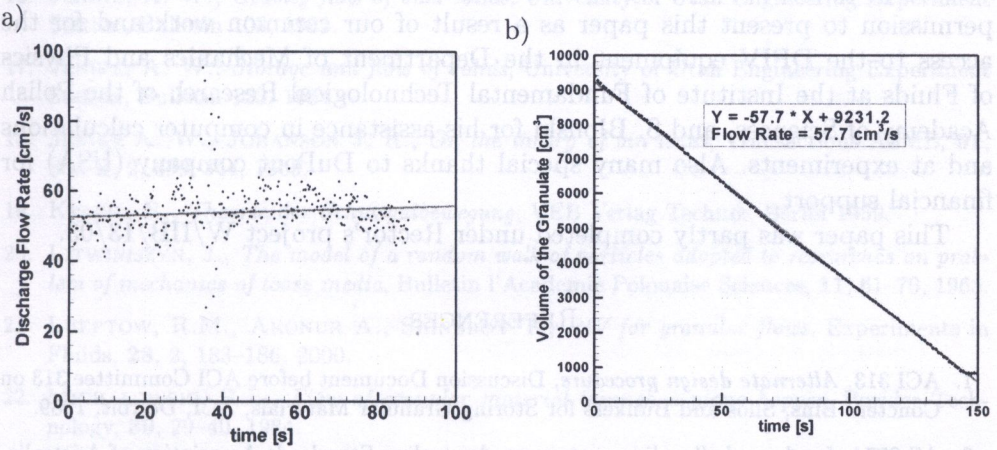

FIG. 16. Volumetric discharge flow rate for flax seed calculated from (a) velocity profiles; (b) measurements of existing volume of the material in the model.

5. CONCLUSIONS

In this paper the use of a new measurement technique DPIV is presented. The data on the evolution of the flow in central and eccentric flows in two configurations – a plane and a converging model-were shown. Two models of silo were made of plexiglass. Detailed analysis of the flow is enabled thanks the DPIV technique. Velocity vector fields, velocity distribution in two flow modes with a detailed analysis of the influence of the position of the outlet are presented.

Some new results obtained for eccentric discharge were shown in this paper. DPIV technique is a new one for two-dimensional flows. So far used in fluid mechanics and now applied in granular material flow, DPIV appeared as a good diagnostic tool for such analyses. Interesting behaviour of the flowing material and details concerning the eccentric flows were observed and recorded by DPIV. The method enables also to calculate stresses in the flowing material from the data of velocity gradients.

Acknowledgments

This paper is as a result of a few years of experiments and investigations on granular material flows. The author expresses her gratitude to Professor Zenon Mróz of the Institute of Fundamental Technological Research of Polish Academy of Sciences for his discussions and consultations during the time of experiments and Professor Andrew Drescher of the University of Minnesota for his valuable discussion and advice. Many special thanks to Doc. T.A. Kowalewski for his permission to present this paper as a result of our common work and for the access to the DPIV equipment in the Department of Mechanics and Physics of Fluids at the Institute of Fundamental Technological Research of the Polish Academy of Sciences, and S. Błoński for his assistance in computer calculations and at experiments. Also many special thanks to DuPont company (USA) for financial support.

This paper was partly completed under Rector's project W/IIB/13/03.

References

1. ACI 313, *Alternate design procedure,* Discussion Document before ACI Committee 313 on Conctere Bins, Silos and Bunkers for Storing Granular Materials, ACI, Detroit, 1989.
2. AS 3774, *Loads on bulk solids containers*, Australian Standards Association of Australia, Sydney, 1986.
3. ASAE EP433, *Loads exerted by free-flowing grains on bins*, ASAE Engineering Practice EP433, ASAE Standards, 1997.
4. Ayuga F., Guaita M., Aguado P.J., Couto A., *Discharge and the eccentricity of the hopper influence on the silo wall pressures*, J. Eng. Mechanics, **127**, 10, 1067–1074, 2001.
5. Blair-Fish P.M., Bransby P.L., *Flow patterns and wall stresses in a mass-flow bunker*, Journal of Engineering for Industry, **95**, 17–26, 1973.
6. Blight G.E, *Eccentric emptying of a large coal bin with six outlets*, Bulk Solids Handling, **11**, 2, 451–457, 1991.
7. Böhrnsen, J.U., Antes, H., Ostendorf, M., Schwedes, J., *Silo discharge: Measurement and Simulation of Dynamic Behaviour in Bulk Solids*, Chem. Eng. Technol., **27**, 71–76, 2004.

8. Borcz A., el Rahim Hamdy Abd, *Wall pressure measurements in eccentricity discharged cement silos*, Bulk Solids Handling, **11**, 2, 469–476, 1991.

9. Carson J. W., *Silo failures: Case histories and lessons learned*, Third Israeli Conference for Conveing and Handling of Particulate Solids, Dead Sea. Israel, May, 2000.

10. Cleaver, J. A. S., Nedderman, R. M., *The measurement of velocity distributions in conical hoppers*, Chemical Engineering Science, **48**, 21, 3693–3703, 1993.

11. Drescher, A., Cousens, T.W., Bransby, P.L., *Kinematics of the mass flow of granular material through a plane hopper*, Geotechique, **28**, 1, 27–42, 1978.

12. Drescher, A, *Analytical methods in bin-load analysis*, Elsevier, Amsterdam 1991.

13. Drescher, A., Ferjani, M., *Revised model for plug/funnel flow in bins*, Powder Technology, **141**, 44–54, 2004.

14. ENV 1991-Part 4 Eurocode 1, *Basis of design and actions on structures. Part 4, Actions on silos and tanks*, Brussels, Belgium 1995.

15. Giunta, J.S., *Flow patterns of granular materials in flat-bottom bins*, Journal of Engineering for Industry, Transactions of the ASME, **91**, 406–413, 1969.

16. Jenike, A. W., *Gravity flow of bulk solids*, University of Utah Engineering Experiment Station, Bulletin 108, 1961.

17. Jenike, A. W., *Storage and flow of solids*, University of Utah Engineering Experiment Station, Bulletin 123, 1964.

18. Jenike A. W., Johanson J. R., *On the theory of bin loads*, Transactions ASME, **91**, Ser. B, 2, 339–344, 1969.

19. Kvapil, R., *Theorie der Schuttgutbewegung*, VEB Verlag Technik, Berlin 1959.

20. Litwiniszyn, J., *The model of a random walk of particles adopted to researches on problem of mechanics of loose media*, Bulletin l'Academie Polonaise Sciences, **11**, 61–70, 1963.

21. Lueptow, R.M., Akonur A., Shinbrot T., *PIV for granular flows*, Experiments in Fluids, **28**, 2, 183–186, 2000.

22. Michałowski, R.L., *Flow of granular material through a plane hopper*, Powder Technology, **39**, 29–40, 1984.

23. Michałowski, R.L., *Flow of granular media through a plane parallel/converging bunker*, Chemical Engineering Science, **42**, 11, 2587–2596, 1987.

24. Molenda M., Horabik J., Thompson S. A., Ross I. J., *Bin loads induced by eccentric filling and discharge of grain*, Tansactions of the ASAE, **45**, 3, 781–785, 2002.

25. Molenda M., Horabik J., *Physical properties of granular alimentary materials*, Acta Agrophysica, Insitute of Agrophysic, Polish Academy of Sciences, Lublin 2002.

26. Moreea, S.B.M., Nedderman, R.M, *Exact Stress and velocity distributions in a cohesionless material discharging from a conical hopper*, Chemical Engineering Sciences, **51**, 16, 3931–3942, 1996.

27. Mróz Z., Szymański C., *Simplified theory of granular material flow in converging channels*, Arch. Inż. Ląd., **17**, 551–578, 1971.

28. Mullins, W. W., *Critique and comparison of two stochastic theories of gravity-induced particle flow*, Powder Technology, **23**, 115–119, 1979.

29. MULLINS, W. W., *Stochastic theory of particle flow under gravity*, Journal of Applied Physics, **43**, 665–677, 1972.

30. NEDDERMAN, R. M., TÜZÜN, U., *A kinematic model for the flow of granular materials*, Powder Technology, **22**, 243–253, 1979.

31. NEDDERMAN, R. M., *Measurement of the velocity profile in a granular material discharging from a conical hopper*, Chemical Engineering Science, **43**, 7, 1507–1516, 1988.

32. NEDDERMAN, R. M., *The use of the kinematic model to predict the development of the stagnant zone boundary in the batch discharge of a bunker*, Chemical Engineering Science, **50**, 6, 959–965, 1995.

33. NGUYEN, T.V., BRENNEN, C., SABERSKY, R.H., *Gravity flow of granular materials in conical hoppers*, Journal of Applied Mechanics, Transactions of the ASME, **46**, 529–535, 1979.

34. OSTENDORF, M., SCHWEDES, J., *Application of optical measurement techniques on the investigation of bulk solids flow behaviour in silos*, Int. Congress for Particle Technology, Partec 2004, Nurnberg, Germany, 16–18 March, 2004.

35. PARISEAU, W.G., *Discontinuous velocity fields in gravity flows of granular materials through slots*, Powder Technology, **3**, 218–226, 1969/70.

36. PITMAN, E. B., *Stress and Velocity fields in two- and three dimensional hoppers*, Powder Technology, **47**, 219–231, 1986.

37. POLDERMAN H.G., SCOTT A.M., BOOM J., *Solids stresses in bunkers with inserts*, Int. Chem. Engng. Symp. Ser., 91, 227–240, 1985.

38. QUENOT, G. M., PAKLEZA, J., KOWALEWSKI, T. A., *Particle image velocimetry with optical flow*, Experiments in Fluids, **25**, 177–189, 1998.

39. ROTTER, J.M., *The analysis of steel bins subject to eccentric discharge. Proc.*, 2-nd Inter. Conference on Bulk Materials Storage Handling and Transportation, Ins. of Eng., Wollongong, Australia, July, 264–271, 1986.

40. ROTTER, J.M., *Guide for the economic design of metal silos*, E&FN Spon, London, 1998.

41. SIELAMOWICZ, I., KOWALEWSKI, T.A., *DPIV technique in modeling granular material flows in a model of silo made of Plexiglass*, Int. Congress for Particle Technology, Partec 2004, Nurnberg, Germany, 16–18 March, 2004.

42. SIELAMOWICZ I., KOWALEWSKI T.A., BŁOŃSKI S., *Central and eccentric granular material flows in bins/hoppers recorded by optical technique DPIV*, Acta Agrophysica, **4**, 2, 2004.

43. SIELAMOWICZ I., BŁOŃSKI S., *Particle image velocimetry analysis of granular material flows*, XXI International Congress of Theoretical and Applied Mechanics, Warsaw, 15–21 August, 2004.

44. SIELAMOWICZ I., BŁOŃSKI S. and KOWALEWSKI T.A., *Optical technique DPIV in measurements of granular material flows, Part 1 of 3-plane hoppers*, Chemical Engineering Science, **60**, 2, 589–598, 2005.

45. TAKAHASHI, H., YANAI, H., *Flow profile and void fraction of granular solids in a moving bed*, Powder Technology, **7**, 205–214, 1973.

46. TÜZÜN, U., NEDDERMAN, R.M., *Investigation of the flow boundary during steady-state discharge from a funnel-flow bunker*, Powder Technology, **31**, 1, 27–43, 1982.

47. TÜZÜN, U., HOULSBY, G. T., NEDDERMAN, R.M., SAVAGE, S.B., *Flow of granular materials - 2. Velocity distributions in slow flow*, Chemical Engineering Science, **37**, 12, 1691–1709, 1982.

48. WALKER, D. M., *An approximate theory for pressures and arching in hoppers*, Chemical Engineering Science, **21**, 975–997, 1966.

49. WATERS, A.J., DRESCHER, A., *Modeling plug flow in bins/hoppers*, Powder Technology, **113**, 168–175, 2000.

50. WATSON G.R., *Flow patterns in flat-bottomed silos*, Ph. D. thesis, University of Edinburgh, 1993.

51. WATSON, G. R., ROTTER J. M., *A finite element kinematic analysis of planar granular solids flow*, Chemical Engineering Science, **51**, 3967–3978, 1996.

52. WEIR, G., J., *A mathematical model for dilating, non-cohessive granular flows in steep-walled hoppers*, Chemical Engineering Science, **59**, 149–161, 2004.

Received January 5, 2005; revised version April 14, 2005.

Erratum

to the paper: I. Sielamowicz *"Experimental analysis of granular material flows using the technique of digital particle image velocimetry"* Engng. Trans., **53**, 2, page 210, 2005

a) Velocity vectors and velocity contours for the time $t = 45$ s

b) Traces of individual particles for the time $t = 45$ s

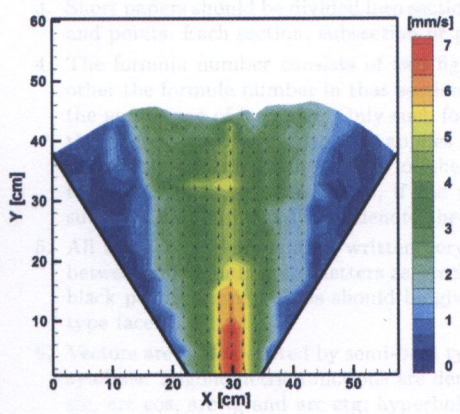

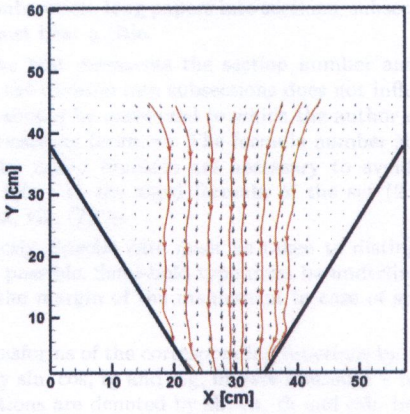

c) Velocity vectors and velocity contours for the time $t = 95$ s

d) Traces of individual particles for the time $t = 95$ s

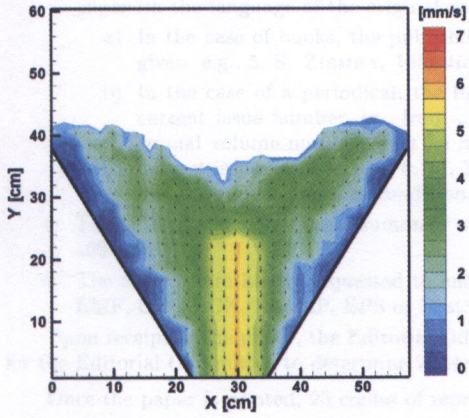

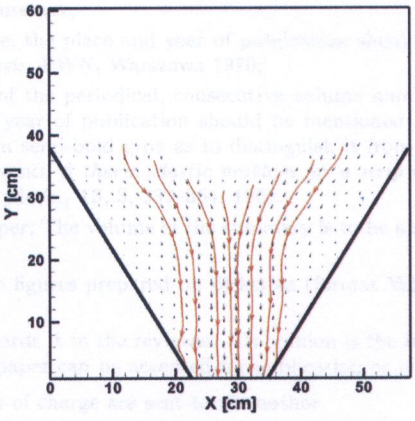

Fig. 7. Velocity contours and traces of individual particles for the flow of amaranthus in the converging model.